The leucine and ATP-induced *in vitro* interaction of LARS1 and RagD was significantly decreased in LARS1 R517A, N802C/G889C, and A888P/G889P mutants compared with WT (Figure 6E), and cells expressing these mutants showed decreased leucine-dependent mTORC1 stimulation on the basis of co-precipitation of RagD with LARS1, the amounts of RagB and RagD precipitated with GTP-agarose beads, and the phosphorylation patterns of S6K in response to leucine (Figures 6F and 6G), suggesting the importance of the R-lever and swing helix rotation for the leucine-dependent RagD association to LARS1.

Although we mutated LARS1 on the basis of structural information to perturb leucine binding, ATP binding, and conformational changes, respectively, all of the mutants lost stimulatory activity for the mTORC1 pathway. To exclude that possible misfolding of the proteins would result in their loss of function, we compared the intrinsic tryptophan fluorescence of LARS1 WT with mutants. The leucine binding-deficient (Y52A/Y54A/H91A), ATP binding-deficient (H60A/H63A), and R-lever movement-deficient (R517A and H251A/R517A) and one of the swing helix movement-deficient (N802C/G889C) mutants showed similar fluorescence ratio at 350 nm/330 nm around physiological temperature, whereas LARS1 WT denatured by boiling showed a much lower value (Figures S6A and S6B). On the other hand, the other swing helix movement-deficient mutant (A888P/G889P) showed slightly different patterns. Because proline has the rigid side chain, there would be possible local misfolding of the protein (Figure S6B). We also examined whether ectopic expression of LARS1 WT or mutants would induce the unfolded protein response (UPR) (Walter and Ron, 2011). LARS1 mutants did not induce UPR markers compared with LARS1 WT, while Brefelin A (BFA) effectively increase the level of binding immunoglobulin protein (BiP) and activating transcription factor 4 (ATF4) (Figure S6C), suggesting that LARS1 mutants were not significantly misfolded.

Structural difference of LARS1 RBD in sensing-on and sensing-off states

To gain insight into how leucine binding to LARS1 could facilitate the association of RagD, we compared the RBDs of the two distinct states. We performed reductive lysine methylation in LARS1's 111 lysine residues (Walter et al., 2006) to acquire more information about disordered regions of the LARS1-Leu-AMS^{syn} RBD and obtained the fourth crystal of LARS1 with Leu-AMS (LARS1^{methyl}-Leu-AMS^{syn}; PDB: 6KR7). Although we cannot suggest the exact mechanism how LARS1-Leu^{syn} is preferred for RagD binding compared with LARS1-Leu-AMS^{syn} at present, the RBD of LARS1-Leu^{syn} is rotated toward the CD compared with that of LARS1^{methyl}-Leu-AMS^{syn}, and the secondary structure compositions are changed, which would be correlated with RagD association (Figure 7A).

Model of LARS1 leucine sensing to RagD association

The R-lever in CP1 hairpin motif and swing helix appear to play a crucial role in the functional switch of LARS1. The serial structural changes of LARS1 from sensing-off to sensing-on are as follows (Figure S7): first, leucine first binds to ^{50}FPYPY^{54} motif ("sensing key sequence"). Second, H251 in CP1 hairpin motif forms a hydrogen bond with the oxygen atom of Y54 and the side chain of R517 (R-lever) protrudes outward, forming a hydrogen bond with D244. (In contrast, in the sensing-off structure, H251 forms a hydrogen bond with R517. R517 appears to move about 11 Å from one state to the other, on the basis of the CZ atom of R517 (Figure 5L). Third, an alternation occurs in hydrogen-bonding networks of CD and CP1, which includes H251 and R517. Forth, swing helix is rotated about 25°, which shifts the LVβ. Finally, the RBD accommodates RagD binding.

DISCUSSION

In summary, LARS1 can adopt two distinct conformational states, only one of which is preferred to interact with RagD, and the transition between the two states is mediated along with LARS1's catalytic activity. Upon leucine binding to the synthetic site, conformation of LARS1 is changed to "sensing-on^{+}" status, and subsequent ATP binding appears to augment leucine binding to more active "sensing-on^{++}" status, although the exact structure is to be determined (Figure 7B). "Sensing-on^{++}" LARS1 would interact with RagD for mTORC1 activation and then would be changed back to "sensing-off" status, releasing RagD when Leu-AMP is generated from leucine and ATP. LARS1 can then bind to tRNA and mediate covalent ligation to make Leu-tRNA-^{Leu}, which is used for proteins synthesis. Although the involvement of intramolecular coupling in conformational change was not completely excluded considering the different unit cells and crystal packing (Table S1), the results of various biochemical and cell-based assays consistently support the R-lever hypothesis. Taken together, we provided the molecular evidence as to how leucine binding to the synthetic site of LARS1 is wired to

Figure 5. Comparison of sensing-off and sensing-on states of LARS1 conformation

(A and B) Two states of LARS1 with leucine-binding (sensing-on^{+}) and Leu-AMS-binding (sensing-off) in the synthetic site. In the text, LARS1 bound with both leucine and ATP in the synthetic site is marked as sensing-on^{2+}. Leu^{CP1} is shown as green, while Leu^{syn} and Leu-AMS^{syn} are cyan. The CP1 hairpin, swing helix, and RBD of the LARS1 CTD are colored as Figures 1A and 1B.

(C–F) Zoomed view of the synthetic sites of LARS1 (C and E) and the junction region between the CD and CP1 hairpin motif (D and F). Leu-AMS^{syn} and Leu^{syn} are represented as cyan sphere models. The residues located in the CP1 hairpin motif and CD are shown as green and blue, respectively. R517, the key residue discriminating sensing-on and sensing-off states, is the magenta stick model. The residues involved in the hydrogen-bonding network (black dotted lines) within 3.5 Å are represented as a stick model.

(G and H) HEK293T cells expressing LARS1 WT and mutants were starved of leucine and then stimulated with leucine. The effects of LARS1 WT and mutants on the leucine-dependent interaction with RagD (upper), conversion of RagD-GTP to RagD-GDP (middle), and S6K phosphorylation patterns (lower) were determined (G). Immunoblot images are representative of three biological replicates. The band intensity of immunoblot images was quantified using Multi Gauge (H) ($n = 3$; mean ± SEM). $^{**}p < 0.01$ and $^{***}p < 0.001$, two-way ANOVA.

(I–L) The structures of LARS1 complexed with Leu (magenta, sensing-on^{+}) (I), ATP (blue, sensing-off^{ATP}) (J), and Leu-AMS (green, sensing-off$^{Leu\text{-}AMS}$) (K) around the ^{50}FPYPY^{54}, H251, and R517 region and their superimposition for comparison (L). Leucine, ATP, and Leu-AMS are represented as yellow stick models.

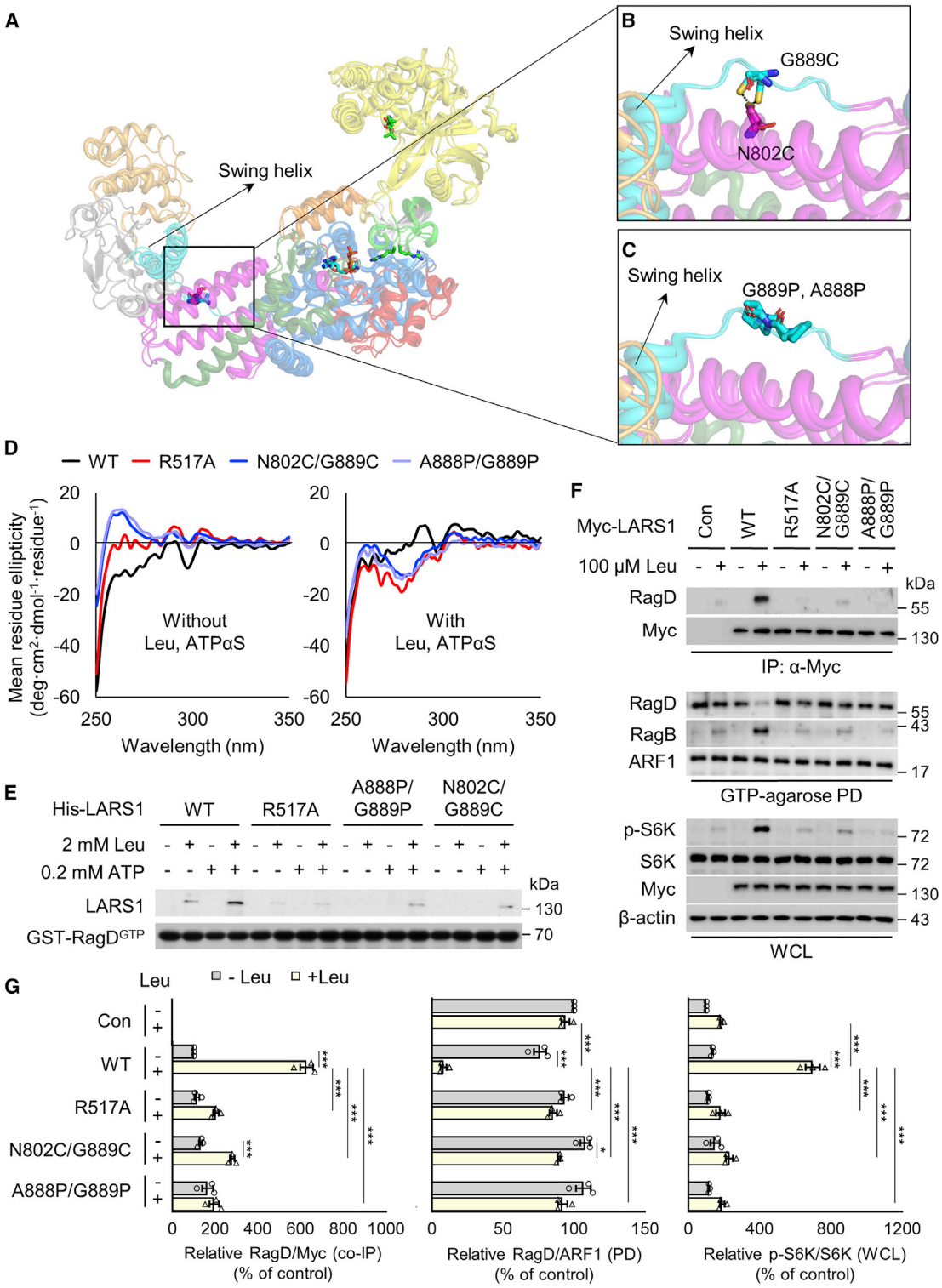

Figure 6. R-lever movement and swing helix rotation for the association of LARS1 with RagD

(A) Superimposed structures of LARS1-Leu^{syn} and LARS1-Leu-AMS^{syn}. The domain color scheme is the same as in Figures 1A and 1B. Leucine, Leu-AMS, R517, N802, A888, and G889 residues are represented by stick models.

(B and C) Zoomed view of model structure around connecting loop between the swing helix and the CD. Substitutions of N802 and G889 to cysteine (B) and G889 and A888 to proline (C) are shown.

(legend continued on next page)

accommodate RagD interaction in the CTD by suggesting leucine-dependent "R-lever" model. Upon binding with leucine and ATP, the R517 residue of LARS1 could be pulled (like a toy vending machine) and then the swing helix rotates to make the RBD more accessible to RagD (Figure 7C).

The recently reported structures of the C-terminal 106 amino acid truncated LARS1 (1–1,070 aa) complexed with Leu-AMS in the synthetic site and Nva2AA in the editing site (PDB: 6LPF), and also with Leu-AMS in the synthetic site and AN6426-AMP in the editing site (PDB: 6LR6), show clear electron density in the CTD, including RBD. Modeling LARS1-tRNA complex on the basis of *Ph*LARS-tRNA complex (PDB: 1WZ2) provided insight into the mutually exclusive relationship of tRNA and RagD in LARS1 binding (Liu et al., 2020). However, it provides little information on the leucine-sensing mechanism of LARS1 for control of the mTORC1 signal pathway. Here we suggest an "R-lever model" for rotation of the CTD as a potential mechanism for leucine-mediated control of LARS1 interaction with RagD for mTORC1 activation. Superposition of the full-length LARS1-Leu^{syn} with the full-length LARS1-Leu-AMS^{syn} (in this work) and C-terminal truncated LARS1-Leu-AMS^{syn} structures shows 25° (Figures 5A and 5B) and 23° (Figure S4A) rotation angles of swing helix, respectively, despite the difference in crystal packing. These results further support the proposed "R-lever model" to control the RBD movement for RagD interaction.

Despite our repeated effort to obtain crystals of LARS1 in complex with both leucine and ATPαS in the synthetic site for providing structural evidence on ATP's role on leucine binding to LARS1, we failed and could just obtain LARS1 crystals with only ATP in the synthetic site (LARS1-ATP^{syn}) (Figure 4A). Unlike the expected conformation of LARS1 in complex with both leucine and ATP in the synthetic site, LARS1-ATP^{syn} showed sensing-off conformation on the basis of the orientation of R-lever (Figures 5J and 5L), consistent with the result that ATP-dependent increase in LARS1-RagD interaction is observed only in the presence of leucine (Figure 3D).

Steady-state cytosolic concentration of ATP is known to range from 0.5 to 5 mM in various cell types (Gribble et al., 2000; Larcombe-McDouall et al., 1999). Considering that even 1 mM ATP seems to be enough to facilitate leucine binding to LARS1 (Figure 3C), the exact physiological significance for ATP occupation in LARS1 to control leucine binding affinity must be further investigated. Nevertheless, the ATP binding-mediated increase in leucine-binding affinity still seems to be applied to physiological conditions. A recent study reported that glucose starvation-induced phosphorylation of LARS1 at the residue crucial for ATP binding results in decreased ATP-binding affinity and then decreased leucine binding affinity (Yoon et al., 2020), suggesting the physiological significance of ATP binding to leucine binding capability of LARS1.

Although we showed a potential leucine-sensing mechanism of LARS1 by determining structural changes of LARS1 upon binding to different substrates and the impact of these changes to the RagD association, we do not yet know how LARS1 could facilitate the conversion of RagD-GTP to RagD-GDP. Determining the complex structures of LARS1 with RagD would be necessary for full understanding how leucine-induced conformational changes of LARS1 are wired to the activation of RagD GTPase.

STAR★METHODS

Detailed methods are provided in the online version of this paper and include the following:

- KEY RESOURCES TABLE
- RESOURCE AVAILABILITY
  - Lead contact
  - Materials availability
  - Data and code availability
- EXPERIMENTAL MODEL AND SUBJECT DETAILS
  - 293T cells
  - Rosetta 1 (DE3) cells
- METHOD DETAILS
  - Cloning, expression, and purification of LARS1
  - Crystallization of LARS1 and structural data collection
  - Structure determination
  - Binding affinity measurement by microscale thermophoresis (MST)
  - Leucine starvation and stimulation of cells
  - GTP-agarose pull down assay
  - Leucine binding assay
  - ATP binding assay
  - Isothermal titration calorimetry (ITC)
  - Inflection temperature (T_i) measurement
  - Circular dichroism spectroscopy
  - Thermal shift assay
- QUANTIFICATION AND STATISTICAL ANALYSIS

SUPPLEMENTAL INFORMATION

Supplemental information can be found online at https://doi.org/10.1016/j.celrep.2021.109031.

ACKNOWLEDGMENTS

This work was supported by the Global Frontier Project grant (NRF-M3A6A4-2010-0029785 and 2013M3A6A4044795) of the National Research

(D) Near-UV circular dichroism spectra of LARS1 WT and mutants in the absence (left) or presence (right) of leucine and ATPαS.
(E) The interaction of His-LARS1 WT or the indicated mutants with GST-RagD^{GTP} was monitored using *in vitro* pull-down assay. GST-RagD^{GTP} coupled with GST Sepharose beads was incubated with His-LARS1 WT or mutants in the indicated conditions, and co-precipitation of LARS1 was monitored by immunoblot. Immunoblot images are representative of three biological replicates.
(F and G) HEK293T cells expressing Myc-LARS1 WT and mutants were incubated in the absence of leucine and then stimulated with leucine. Leucine-dependent co-immunoprecipitation of RagD with LARS1 (upper), the amount of GTP-loaded RagD and RagB (middle), and the phosphorylation of S6K patterns (lower) were determined using immunoblot as above (F). Immunoblot images are representative of three biological replicates. The band intensity of immunoblot images was quantified using Multi Gauge (G) (n = 3; mean ± SEM). *p < 0.05 and ***p < 0.001, two-way ANOVA.

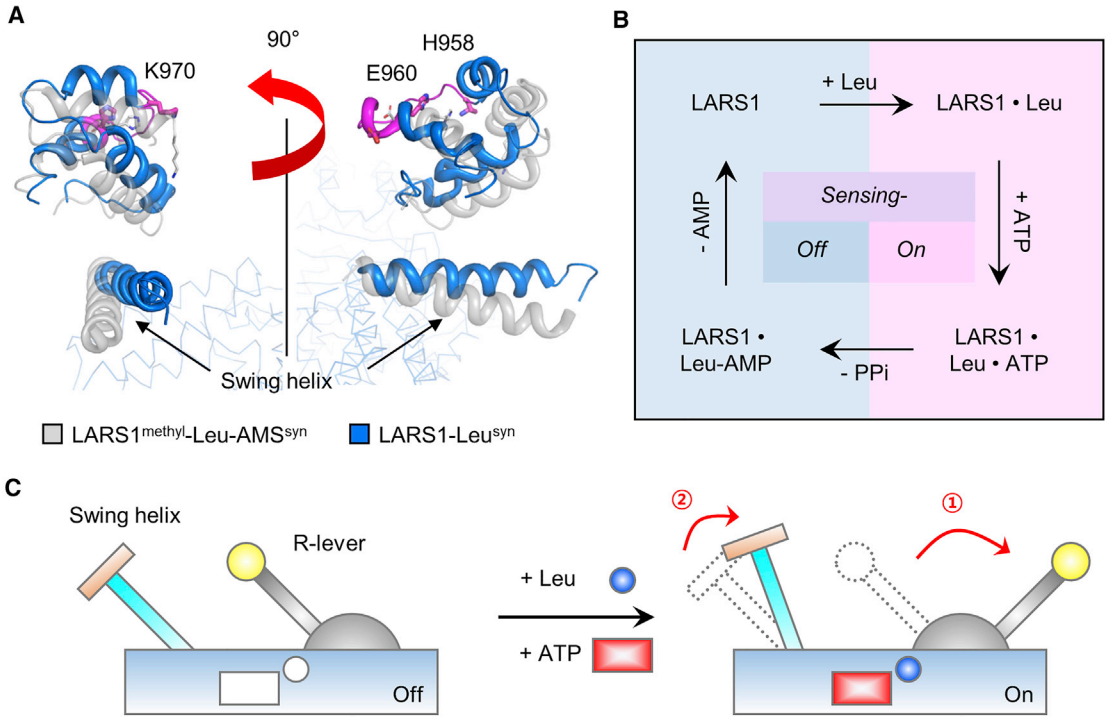

Figure 7. Leucine binding-induced conformational changes of LARS1

(A) Structural comparison between LARS1^{methyl}-Leu-AMS^{syn} and LARS1-Leu^{syn} at the RBD and swing helix. LARS1^{methyl}-Leu-AMS^{syn} structure is colored in gray ribbon model, and LARS1-Leu^{syn} structure is in blue. RagD binding residues (H958, E960, and K970) (Han et al., 2012) are shown as magenta stick models.

(B) Schematic representation of leucine- and ATP-dependent functional transition circuit of LARS1 for mTORC1 activation.

(C) Schematic model of LARS1 conformational changes induced by the association of leucine and ATP.

Foundation (NRF) funded by the Ministry of Science and ICT (MSIT) of Korea, the Yonsei University Research Fund (2020-22-0358), and an NRF grant funded by the Korean government (2018M3A9F3055925, 2020R1A2C2005670, 2020R1I1A1A01067423, 2020R1A2C2099586, and 2020M3E5E2040282). We thank the staff at the PLS 5C, 7A, 11C beamline in South Korea, Photon Factory 1A, and Spring-8 44XU beamline in Japan for the use of their excellent facilities and assistance with X-ray data collection. We also acknowledge the Korean Basic Science Institute (Daejeon, Korea) for the use of a circular dichroism spectrophotometer. Sulhee Kim was supported by the WISET program (2018-644) and NRF-2019R1I1A1A01056 of Korea.

AUTHOR CONTRIBUTIONS

K.Y.H. and Sunghoon Kim designed all experiments. Sulhee Kim cloned, purified, and crystallized WT of LARS1s. J.S. and Sulhee Kim prepared LARS1 mutants. J.S. and Sulhee Kim collected and processed the diffraction data of LARS1s. Sulhee Kim, I.Y., J.P., K.K., J.M.H., J.S., and J.-H.L. performed the biochemical analysis. S.-Y.P., B.S.K., and K.Y.H. determined the crystal structures of LARS1s. I.Y., J.S., Sulhee Kim, Sunghoon Kim, and K.Y.H. analyzed the data and wrote the manuscript.

DECLARATION OF INTERESTS

The authors declare no competing interests.

Received: July 5, 2020
Revised: December 18, 2020
Accepted: April 2, 2021
Published: April 27, 2021

REFERENCES

Adams, P.D., Grosse-Kunstleve, R.W., Hung, L.W., Ioerger, T.R., McCoy, A.J., Moriarty, N.W., Read, R.J., Sacchettini, J.C., Sauter, N.K., and Terwilliger, T.C. (2002). PHENIX: building new software for automated crystallographic structure determination. Acta Crystallogr. D Biol. Crystallogr. *58*, 1948–1954.

Bar-Peled, L., Schweitzer, L.D., Zoncu, R., and Sabatini, D.M. (2012). Ragulator is a GEF for the rag GTPases that signal amino acid levels to mTORC1. Cell *150*, 1196–1208.

Bar-Peled, L., Chantranupong, L., Cherniack, A.D., Chen, W.W., Ottina, K.A., Grabiner, B.C., Spear, E.D., Carter, S.L., Meyerson, M., and Sabatini, D.M. (2013). A tumor suppressor complex with GAP activity for the Rag GTPases that signal amino acid sufficiency to mTORC1. Science *340*, 1100–1106.

Bartoschik, T., Galinec, S., Kleusch, C., Walkiewicz, K., Breitsprecher, D., Weigert, S., Muller, Y.A., You, C., Piehler, J., Vercruysse, T., et al. (2018). Near-native, site-specific and purification-free protein labeling for quantitative protein interaction analysis by microscale thermophoresis. Sci. Rep. *8*, 4977.

Bonfils, G., Jaquenoud, M., Bontron, S., Ostrowicz, C., Ungermann, C., and De Virgilio, C. (2012). Leucyl-tRNA synthetase controls TORC1 via the EGO complex. Mol. Cell *46*, 105–110.

Chantranupong, L., Scaria, S.M., Saxton, R.A., Gygi, M.P., Shen, K., Wyant, G.A., Wang, T., Harper, J.W., Gygi, S.P., and Sabatini, D.M. (2016). The CASTOR proteins are arginine sensors for the mTORC1 pathway. Cell *165*, 153–164.

Cusack, S., Yaremchuk, A., and Tukalo, M. (2000). The 2 A crystal structure of leucyl-tRNA synthetase and its complex with a leucyl-adenylate analogue. EMBO J. *19*, 2351–2361.

Dibble, C.C., and Manning, B.D. (2013). Signal integration by mTORC1 coordinates nutrient input with biosynthetic output. Nat. Cell Biol. *15*, 555–564.

Emsley, P., and Cowtan, K. (2004). Coot: model-building tools for molecular graphics. Acta Crystallogr. D Biol. Crystallogr. *60*, 2126–2132.

Eriani, G., Delarue, M., Poch, O., Gangloff, J., and Moras, D. (1990). Partition of tRNA synthetases into two classes based on mutually exclusive sets of sequence motifs. Nature *347*, 203–206.

Freedman, R., Gibson, B., Donovan, D., Biemann, K., Eisenbeis, S., Parker, J., and Schimmel, P. (1985). Primary structure of histidine-tRNA synthetase and characterization of hisS transcripts. J. Biol. Chem. *260*, 10063–10068.

Fukunaga, R., and Yokoyama, S. (2005a). Aminoacylation complex structures of leucyl-tRNA synthetase and tRNALeu reveal two modes of discriminator-base recognition. Nat. Struct. Mol. Biol. *12*, 915–922.

Fukunaga, R., and Yokoyama, S. (2005b). Crystal structure of leucyl-tRNA synthetase from the archaeon Pyrococcus horikoshii reveals a novel editing domain orientation. J. Mol. Biol. *346*, 57–71.

Gribble, F.M., Loussouarn, G., Tucker, S.J., Zhao, C., Nichols, C.G., and Ashcroft, F.M. (2000). A novel method for measurement of submembrane ATP concentration. J. Biol. Chem. *275*, 30046–30049.

Gu, X., Orozco, J.M., Saxton, R.A., Condon, K.J., Liu, G.Y., Krawczyk, P.A., Scaria, S.M., Harper, J.W., Gygi, S.P., and Sabatini, D.M. (2017). SAMTOR is an *S*-adenosylmethionine sensor for the mTORC1 pathway. Science *358*, 813–818.

Han, J.M., Jeong, S.J., Park, M.C., Kim, G., Kwon, N.H., Kim, H.K., Ha, S.H., Ryu, S.H., and Kim, S. (2012). Leucyl-tRNA synthetase is an intracellular leucine sensor for the mTORC1-signaling pathway. Cell *149*, 410–424.

Ibba, M., and Soll, D. (2000). Aminoacyl-tRNA synthesis. Annu. Rev. Biochem. *69*, 617–650.

Iyer, G., Hanrahan, A.J., Milowsky, M.I., Al-Ahmadie, H., Scott, S.N., Janakiraman, M., Pirun, M., Sander, C., Socci, N.D., Ostrovnaya, I., et al. (2012). Genome sequencing identifies a basis for everolimus sensitivity. Science *338*, 221.

Jewell, J.L., Kim, Y.C., Russell, R.C., Yu, F.X., Park, H.W., Plouffe, S.W., Tagliabracci, V.S., and Guan, K.L. (2015). Metabolism. Differential regulation of mTORC1 by leucine and glutamine. Science *347*, 194–198.

Johnson, S.C., Rabinovitch, P.S., and Kaeberlein, M. (2013). mTOR is a key modulator of ageing and age-related disease. Nature *493*, 338–345.

Kim, J., and Guan, K.L. (2019). mTOR as a central hub of nutrient signalling and cell growth. Nat. Cell Biol. *21*, 63–71.

Kim, D.H., Sarbassov, D.D., Ali, S.M., King, J.E., Latek, R.R., Erdjument-Bromage, H., Tempst, P., and Sabatini, D.M. (2002). mTOR interacts with raptor to form a nutrient-sensitive complex that signals to the cell growth machinery. Cell *110*, 163–175.

Kim, S., You, S., and Hwang, D. (2011). Aminoacyl-tRNA synthetases and tumorigenesis: more than housekeeping. Nat. Rev. Cancer *11*, 708–718.

Kim, J., Jung, J., Koo, J., Cho, W., Lee, W.S., Kim, C., Park, W., and Park, S.B. (2016). Diversity-oriented synthetic strategy for developing a chemical modulator of protein-protein interaction. Nat. Commun. *7*, 13196.

Kim, J.H., Lee, C., Lee, M., Wang, H., Kim, K., Park, S.J., Yoon, I., Jang, J., Zhao, H., Kim, H.K., et al. (2017). Control of leucine-dependent mTORC1 pathway through chemical intervention of leucyl-tRNA synthetase and RagD interaction. Nat. Commun. *8*, 732.

Kwon, N.H., Fox, P.L., and Kim, S. (2019). Aminoacyl-tRNA synthetases as therapeutic targets. Nat. Rev. Drug Discov. *18*, 629–650.

Larcombe-McDouall, J., Buttell, N., Harrison, N., and Wray, S. (1999). In vivo pH and metabolite changes during a single contraction in rat uterine smooth muscle. J. Physiol. *518*, 783–790.

Lee, M., Kim, J.H., Yoon, I., Lee, C., Fallahi Sichani, M., Kang, J.S., Kang, J., Guo, M., Lee, K.Y., Han, G., et al. (2018). Coordination of the leucine-sensing Rag GTPase cycle by leucyl-tRNA synthetase in the mTORC1 signaling pathway. Proc. Natl. Acad. Sci. U S A *115*, E5279–E5288.

Lei, H.T., Ma, J., Sanchez Martinez, S., and Gonen, T. (2018). Crystal structure of arginine-bound lysosomal transporter SLC38A9 in the cytosol-open state. Nat. Struct. Mol. Biol. *25*, 522–527.

Ling, C., Yao, Y.N., Zheng, Y.G., Wei, H., Wang, L., Wu, X.F., and Wang, E.D. (2005). The C-terminal appended domain of human cytosolic leucyl-tRNA synthetase is indispensable in its interaction with arginyl-tRNA synthetase in the multi-tRNA synthetase complex. J. Biol. Chem. *280*, 34755–34763.

Liu, R.J., Long, T., Li, H., Zhao, J., Li, J., Wang, M., Palencia, A., Lin, J., Cusack, S., and Wang, E.D. (2020). Molecular basis of the multifaceted functions of human leucyl-tRNA synthetase in protein synthesis and beyond. Nucleic Acids Res. *48*, 4946–4959.

Murshudov, G.N., Vagin, A.A., and Dodson, E.J. (1997). Refinement of macromolecular structures by the maximum-likelihood method. Acta Crystallogr. D Biol. Crystallogr. *53*, 240–255.

Nicklin, P., Bergman, P., Zhang, B., Triantafellow, E., Wang, H., Nyfeler, B., Yang, H., Hild, M., Kung, C., Wilson, C., et al. (2009). Bidirectional transport of amino acids regulates mTOR and autophagy. Cell *136*, 521–534.

Otwinowski, Z., and Minor, W. (1997). Processing of X-ray diffraction data collected in oscillation mode. Methods Enzymol. *276*, 307–326.

Palencia, A., Crépin, T., Vu, M.T., Lincecum, T.L., Jr., Martinis, S.A., and Cusack, S. (2012). Structural dynamics of the aminoacylation and proofreading functional cycle of bacterial leucyl-tRNA synthetase. Nat. Struct. Mol. Biol. *19*, 677–684.

Ribas de Pouplana, L., and Schimmel, P. (2001). Two classes of tRNA synthetases suggested by sterically compatible dockings on tRNA acceptor stem. Cell *104*, 191–193.

Rossmann, M.G., Moras, D., and Olsen, K.W. (1974). Chemical and biological evolution of nucleotide-binding protein. Nature *250*, 194–199.

Sancak, Y., Peterson, T.R., Shaul, Y.D., Lindquist, R.A., Thoreen, C.C., Bar-Peled, L., and Sabatini, D.M. (2008). The Rag GTPases bind raptor and mediate amino acid signaling to mTORC1. Science *320*, 1496–1501.

Saxton, R.A., and Sabatini, D.M. (2017). mTOR signaling in growth, metabolism, and disease. Cell *168*, 960–976.

Saxton, R.A., Knockenhauer, K.E., Wolfson, R.L., Chantranupong, L., Pacold, M.E., Wang, T., Schwartz, T.U., and Sabatini, D.M. (2016a). Structural basis for leucine sensing by the Sestrin2-mTORC1 pathway. Science *351*, 53–58.

Saxton, R.A., Chantranupong, L., Knockenhauer, K.E., Schwartz, T.U., and Sabatini, D.M. (2016b). Mechanism of arginine sensing by CASTOR1 upstream of mTORC1. Nature *536*, 229–233.

Shen, K., and Sabatini, D.M. (2018). Ragulator and SLC38A9 activate the Rag GTPases through noncanonical GEF mechanisms. Proc. Natl. Acad. Sci. U S A *115*, 9545–9550.

Son, K., You, J.S., Yoon, M.S., Dai, C., Kim, J.H., Khanna, N., Banerjee, A., Martinis, S.A., Han, G., Han, J.M., et al. (2019). Nontranslational function of leucyl-tRNA synthetase regulates myogenic differentiation and skeletal muscle regeneration. J. Clin. Invest. *129*, 2088–2093.

Sun, H., Kosaras, B., Klein, P.M., and Jensen, F.E. (2013). Mammalian target of rapamycin complex 1 activation negatively regulates Polo-like kinase 2-mediated homeostatic compensation following neonatal seizures. Proc. Natl. Acad. Sci. U S A *110*, 5199–5204.

Tsun, Z.Y., Bar-Peled, L., Chantranupong, L., Zoncu, R., Wang, T., Kim, C., Spooner, E., and Sabatini, D.M. (2013). The folliculin tumor suppressor is a GAP for the RagC/D GTPases that signal amino acid levels to mTORC1. Mol. Cell *52*, 495–505.

Wagle, N., Grabiner, B.C., Van Allen, E.M., Amin-Mansour, A., Taylor-Weiner, A., Rosenberg, M., Gray, N., Barletta, J.A., Guo, Y., Swanson, S.J., et al. (2014). Response and acquired resistance to everolimus in anaplastic thyroid cancer. N. Engl. J. Med. *371*, 1426–1433.

Walter, P., and Ron, D. (2011). The unfolded protein response: from stress pathway to homeostatic regulation. Science *334*, 1081–1086.

Walter, T.S., Meier, C., Assenberg, R., Au, K.F., Ren, J., Verma, A., Nettleship, J.E., Owens, R.J., Stuart, D.I., and Grimes, J.M. (2006). Lysine methylation as a routine rescue strategy for protein crystallization. Structure *14*, 1617–1622.

Wang, S., Tsun, Z.Y., Wolfson, R.L., Shen, K., Wyant, G.A., Plovanich, M.E., Yuan, E.D., Jones, T.D., Chantranupong, L., Comb, W., et al. (2015). Metabolism. Lysosomal amino acid transporter SLC38A9 signals arginine sufficiency to mTORC1. Science *347*, 188–194.

Wienken, C.J., Baaske, P., Rothbauer, U., Braun, D., and Duhr, S. (2010). Protein-binding assays in biological liquids using microscale thermophoresis. Nat. Commun. *1*, 100.

Wolfson, R.L., Chantranupong, L., Saxton, R.A., Shen, K., Scaria, S.M., Cantor, J.R., and Sabatini, D.M. (2016). Sestrin2 is a leucine sensor for the mTORC1 pathway. Science *351*, 43–48.

Yan, W., Tan, M., Eriani, G., and Wang, E.D. (2013). Leucine-specific domain modulates the aminoacylation and proofreading functional cycle of bacterial leucyl-tRNA synthetase. Nucleic Acids Res. *41*, 4988–4998.

Yoon, M.S., Son, K., Arauz, E., Han, J.M., Kim, S., and Chen, J. (2016). Leucyl-tRNA synthetase activates Vps34 in amino acid-sensing mTORC1 signaling. Cell Rep. *16*, 1510–1517.

Yoon, S., Kim, J.H., Koh, Y., Tran, P.T., Ann, J., Yoon, I., Jang, J., Kim, W.K., Lee, S., Lee, J., et al. (2017). Discovery of simplified leucyladenylate sulfamates as novel leucyl-tRNA synthetase (LRS)-targeted mammalian target of rapamycin complex 1 (mTORC1) inhibitors. Bioorg. Med. Chem. *25*, 4145–4152.

Yoon, S., Kim, S.E., Kim, J.H., Yoon, I., Tran, P.T., Ann, J., Kim, C., Byun, W.S., Lee, S., Kim, S., et al. (2019). Structure-activity relationship of leucyladenylate sulfamate analogues as leucyl-tRNA synthetase (LRS)-targeting inhibitors of Mammalian target of rapamycin complex 1 (mTORC1). Bioorg. Med. Chem. *27*, 1099–1109.

Yoon, I., Nam, M., Kim, H.K., Moon, H.S., Kim, S., Jang, J., Song, J.A., Jeong, S.J., Kim, S.B., Cho, S., et al. (2020). Glucose-dependent control of leucine metabolism by leucyl-tRNA synthetase 1. Science *367*, 205–210.

STAR★METHODS

KEY RESOURCES TABLE

REAGENT or RESOURCE	SOURCE	IDENTIFIER
Antibodies		
Rabbit polyclonal anti-phospho-S6K (Thr389)	Cell Signaling Technology	Cat# 9205; RRID:AB_330944
Rabbit polyclonal anti-S6K	Cell Signaling Technology	Cat# 9202; RRID:AB_331676
Rabbit polyclonal anti-RagB	Cell Signaling Technology	Cat# 3830; RRID:AB_1950390
Rabbit polyclonal anti-RagD	Bethyl Laboratories	Cat# A304-301A; RRID:AB_2620497
Rabbit polyclonal anti-LARS1	Bethyl Laboratories	Cat# A304-315A; RRID:AB_2620511
Mouse monoclonal anti-c-Myc (9E10)	Santa Cruz Biotechnology	Cat# sc-40; RRID:AB_390912
Rabbit polyclonal anti-c-Myc	Bethyl Laboratories	Cat# A190-105A; RRID:AB_67390
Mouse monoclonal anti-Flag M2	Sigma-Aldrich	Cat# A1978; RRID:AB_476692
Mouse monoclonal anti-ARF1 (ARFS 1A9/5)	Santa Cruz Biotechnology	Cat# sc-53168; RRID:AB_2060825
Rabbit monoclonal anti-BiP (C50B12)	Cell Signaling Technology	Cat# 3177; RRID:AB_2119845
Rabbit monoclonal anti-ATF-4 (D4B8)	Cell Signaling Technology	Cat# 11815; RRID:AB_2616025
Mouse monoclonal anti-beta-actin (Clone AC-15)	Sigma-Aldrich	Cat# A1978; RRID:AB_476692
Goat anti-mouse IgG (H+L) secondary antibody, HRP	Thermo Fisher Scientific	Cat# 31430; RRID:AB_228307
Goat anti-rabbit IgG (H+L) secondary antibody, HRP	Thermo Fisher Scientific	Cat# 31460; RRID:AB_228341
Bacterial and virus strains		
E. coli: DH5α Competent cells	RBC	Cat# RH618
E. coli: Rosetta 1 (DE3)	Novagen	70954
Chemicals, peptides, and recombinant proteins		
Leu-AMS	This paper	N/A
[2,8-^{3}H]- Adenosine 5'-Triphosphate, tetrasodium salt	PerkinElmer	Cat# NET420250UC
L-[4,5-^{3}H(N)]-Leucine	American Radiolabeled Chemical	Cat# ART0140A-5MCi
Protease inhibitor cocktail	Calbiochem	Cat# 535140
Phosphatase inhibitor cocktail	Thermo Fisher Scientific	Cat# 78427
Leucine-free DMEM	Welgene	Cat# LM001-91
Guanosine 5′-triphosphate-agarose bead	Sigma-Aldrich	Cat# G9768
rProtein G Agarose	Invitrogen	Cat# 15920-010
Glutathione Sepharose 4B	GE Healthcare	Cat# 17-0756-01
L-Leucine solution	Welgene	Cat# LS042-01
TurboFect	Thermo Fisher Scientific	Cat# R0531
LB broth	Merck Millipore	Cat# 1102855000
Agar	Duchefa	Cat# M1002.1000
Ampicillin	Duchefa	Cat# A0104.0025
Chloramphenicol	Sigma-Aldrich	Cat# C0378-100G
IPTG	Duchefa	Cat# I1401.0025
L-Leucine	Sigma-Aldrich	Cat# L8000-100G
L-Isoleucine	Sigma-Aldrich	Cat# I2752-100G
L-Valine	Sigma-Aldrich	Cat# V0500-100G
L-Tryptophan	Sigma-Aldrich	Cat# T0254-100G

(*Continued on next page*)

Continued

REAGENT or RESOURCE	SOURCE	IDENTIFIER
2-Mercaptoethanol	Sigma-Aldrich	Cat# M3148-250ML
Tween20	Sigma-Aldrich	Cat# P1379-1L
Imidazole	Biobasic	Cat# IB0277 −500G
Hydrochloric acid	Samchun	Cat# H0255
Sodium hydroxide	Samchun	Cat# S0610
DTT	Duchefa	Cat# D1309.0025
TRIS	Duchefa	Cat# T1501.5000
HEPES	Merck Millipore	Cat# 391338-1KGCN
PBS	Sigma-Aldrich	Cat# P3813
Sodium chloride	Duchefa	Cat# S0520.5000
Magnesium chloride	Duchefa	Cat# M0533.1000
Formaldehyde	Sigma-Aldrich	Cat# F8775-25ML
Borane dimethylamine complex	Sigma-Aldrich	Cat# 180238-25G
Bis-tris (pH6.5)	Hampton research	Cat# HR2-783
Ammonium sulfate	Hampton research	Cat# HR2-541
HEPES	Hampton research	Cat# HR2-585
PEG3350	Hampton research	Cat# HR2-527
Sodium hydroxide	Hampton research	Cat# HR2-583
ATP	Sigma-Aldrich	Cat# A2383-25G
ATPαS	Jena Bioscience	Cat# NU-408L
Deposited data		
Structure of human LARS1-Leu^{syn}	This paper	PDB: 6KQY
Structure of human LARS1-ATP^{syn}	This paper	PDB: 6KID
Structure of human LARS1-Leu-AMS^{syn}	This paper	PDB: 6KIE
Structure of human LARS1^{methyl}-Leu-AMS^{syn}	This paper	PDB: 6KR7
Structure of human cytoplasmic LRS with Leu-AMS and Nva2AA	Liu et al., 2020	PDB: 6LPF
Structure of human cytoplasmic LRS with Leu-AMS and AN6426-AMP	Liu et al., 2020	PDB: 6LR6
Structure of *Pyrococcus horikoshii* LARS	Fukunaga and Yokoyama, 2005b	PDB: 1WKB
Experimental models: Cell lines		
Human: 293T cells	ATCC	Cat# CRL-3216; RRID:CVCL_0063
Recombinant DNA		
Plasmid: pQE-80L-His-LARS1	Han et al., 2012	N/A
Plasmid: pQE-80L-His-LARS1 Y52A/Y54A/H91A	This paper	N/A
Plasmid: pQE-80L-His-LARS1 H60A/H63A	This paper	N/A
Plasmid: pQE-80L-His-LARS1 E257A	This paper	N/A
Plasmid: pQE-80L-His-LARS1 R517A	This paper	N/A
Plasmid: pQE-80L-His-LARS1 H251A/R517A	This paper	N/A
Plasmid: pQE-80L-His-LARS1 N802C/G889C	This paper	N/A
Plasmid: pQE-80L-His-LARS1 A888P/G889P	This paper	N/A
Plasmid: pcDNA3	Han et al., 2012	N/A
Plasmid: pcDNA3-Myc-LARS1	Han et al., 2012	N/A
Plasmid: pcDNA3-Myc-LARS1 Y52A/Y54A	This paper	N/A

(*Continued on next page*)

Continued

REAGENT or RESOURCE	SOURCE	IDENTIFIER
Plasmid: pcDNA3-Myc-LARS1 H91A	This paper	N/A
Plasmid: pcDNA3-Myc-LARS1 Y52A/ Y54A/H91A	This paper	N/A
Plasmid: pcDNA3-Myc-LARS1 H60A/H63A	This paper	N/A
Plasmid: pcDNA3-Myc-LARS1 E257A	This paper	N/A
Plasmid: pcDNA3-Myc-LARS1 S673A/ D676A	This paper	N/A
Plasmid: pcDNA3-Myc-LARS1 H251A	This paper	N/A
Plasmid: pcDNA3-Myc-LARS1 R517A	This paper	N/A
Plasmid: pcDNA3-Myc-LARS1 H251A/ R517A	This paper	N/A
Plasmid: pcDNA3-Myc-LARS1 N802C/ G889C	This paper	N/A
Plasmid: pcDNA3-Myc-LARS1 A888P/ G889P	This paper	N/A
Plasmid: pGEX4T3-GST-RagD Q121L	This paper	N/A
Software and algorithms		
Multi Gauge V3.0	Fujifilm	Fujifilm
Prism 9	GraphPad	https://www.graphpad.com/scientific-software/prism/
HKL2000	Otwinowski and Minor, 1997	https://www.hkl-xray.com/
AutoSol	Adams et al., 2002	https://www.phenix-online.org
PHENIX	Adams et al., 2002	https://www.phenix-online.org
Phaser	Adams et al., 2002	https://www.phenix-online.org
COOT	Emsley and Cowtan, 2004	https://www2.mrc-lmb.cam.ac.uk/personal/pemsley/coot
PyMol	PyMol	http://www.pymol.org/2/
Monolith NT.115	MO.Affinity Analysis v2.3	NanoTemper Technologies, Munich, Germany
Tycho NT.6	Tycho Analysis	NanoTemper Technologies, Munich, Germany
Affinity ITC	NanoAnalyze program	TA Instruments
Circular dichroism spectroscopy	J715 spectropolarimeter	JASCO corporation
Other		
HisTrap HP	GE Healthcare	17-5248-02
HiTrap Q FF	GE Healthcare	17-5156-01
HiLoad 26/600 Superdex 200 pg	GE Healthcare	28-9893-36
Amicon Ultra Centrifugal Filter	Merck Millipore, GE	UFC903096

RESOURCE AVAILABILITY

Lead contact

Further information and requests for resources and reagents should be directed to the Lead contact, Sunghoon Kim (sunghoonkim@yonsei.ac.kr).

Materials availability

Materials generated in this study are available upon request.

Data and code availability

All data are available in the main text or supplementary information. The accession numbers for the structures of LARS1-Leu^{syn}, LARS1-ATP^{syn}, LARS1-Leu-AMS^{syn}, and LARS1^{methyl}-Leu-AMS^{syn} reported in this paper are PDB: 6KQY, PDB: 6KID, PDB: 6KIE, and PDB: 6KR7, respectively.

EXPERIMENTAL MODEL AND SUBJECT DETAILS

293T cells

293T cells were obtained from American Type Culture Collection (ATCC). The cells were grown in Dulbecco's Modified Eagle Medium (Hyclone), supplemented with penicillin-streptomycin (Hyclone) and 10% heat inactivated fetal bovine serum (Hyclone).

Rosetta 1 (DE3) cells

Rosetta 1 (DE3) cells were obtained from Novagen.

METHOD DETAILS

Cloning, expression, and purification of LARS1

LARS1 cDNA was cloned into pQE-80L (Quiagen) and the recombinant plasmid was transformed into *Escherichia coli* Rosetta 1 (DE3) (Novagen). The cells were grown at 37°C in Luria-Bertani medium until the optical density at 600 nm reached 0.6 - 0.8. The recombinant protein was induced by the addition of 0.5 mM isopropyl-β-D-1-thiogalactopyranoside at 18°C for 18 hr. The cells were harvested by centrifugation at 4,500 *g* for 20 min at 4°C. The harvested cell pellet was resuspended in Buffer A containing 20 mM Tris (pH 8.0), 150 mM NaCl, 5 mM $MgCl_2$, 5 mM β-mercaptoethanol, and 0.1% Tween 20. The cell lysates were disrupted by sonication and the soluble fraction was obtained by centrifuging at 24,878 *g* for 1 hr at 4°C. The supernatant was filtered with a 0.45 μm pore-sized membrane and then loaded onto a Ni^{2+}-affinity column (HisTrap HP 5 ml, GE Healthcare) that was pre-equilibrated with Buffer A. The recombinant proteins bound on the column were eluted with a linear gradient of Buffer A containing 500 mM imidazole. The pooled fractions were diluted with Buffer B containing 20 mM Tris (pH 8.0), 2 mM DTT, and 0.1% Tween 20 up to 10 times, and the resulting proteins were further purified by anion exchange chromatography using a linear gradient of Buffer B containing 1 M NaCl. Finally, size-exclusion chromatography was conducted using a HiLoad 26/60 Superdex 200 prep-grade column with Final Buffer (20 mM Tris-HCl (pH 7.5), 150 mM NaCl, 5 mM $MgCl_2$, 2 mM DTT and 0.1% Tween 20), and the fractions containing the recombinant proteins were pooled. The pooled proteins were concentrated to 30 mg/ml using an Amicon Ultra Centrifugal Filter (Merck Millipore, GE) and then stored at - 80°C. Purification of LARS1 mutants was carried out as described above except for LARS1 N802C/G889C. LARS1 N802C/G889C was purified in the absence of DTT in all steps.

Crystallization of LARS1 and structural data collection

Initial crystallization was performed at 20°C using the sitting-drop vapor diffusion method with MRC 2 Well Crystallization Plates (Hampton Research). The purified full-length LARS1 was incubated with different molecules (2 mM leucine for LARS1-Leu^{syn}), 2 mM leucine and 1 mM ATP for LARS1-ATP^{syn}), 2 mM leucine and 1 mM Leu-AMS for LARS1- Leu-AMS^{syn}), and 2 mM leucine and 1 mM Leu-AMS for $LARS1^{methyl}$-Leu-AMS^{syn})) for 1 hr prior to crystallization. The suitable crystals of LARS1-Leu^{syn} for X-ray diffraction were obtained by mixing 1 μL of ~25 mg/ml protein in 20 mM Tris-HCl (pH 7.5), 150 mM NaCl, 5 mM $MgCl_2$, 2 mM DTT, and 0.1% Tween 20 with 1 μL of a reservoir solution containing 0.1 M bis-tris (pH 6.5), 1.60 M Ammonium sulfate at 20°C using hanging-drop vapor diffusion method. The suitable crystals of LARS1-ATP^{syn}, LARS1-Leu-AMS^{syn}, and $LARS1^{methyl}$-Leu-AMS^{syn} for X-ray diffraction were obtained by mixing 1 μL of ~17 mg/ml protein in 20 mM Tris-HCl (pH 7.5), 150 mM NaCl, 5 mM $MgCl_2$, 2 mM DTT, and 0.1% Tween 20 with 1 μL of a reservoir solution containing 0.1 M HEPES (pH 7.1), 0.42 M Ammonium sulfate, and 24% PEG3350 at 20°C using hanging-drop vapor diffusion method. A day before transfer to liquid nitrogen, the crystals of LARS1-Leu^{syn} were moved to the cryoprotectant solution containing 25% glycerol in the best optimized crystal reservoir condition and then frozen at −20°C for the stabilization. All crystals were transferred to a cryoprotectant solution containing 25% glycerol in reservoir solution and then immediately flash-frozen in liquid nitrogen. Diffraction datasets were collected using Pohang Accelerator Light Source beamline (5C, 7A, and 11C) (Pohang, South Korea), beamline BL44XU at the SPring-8 (Japan), and beamline BL1A at Photon Factory (Japan). The dataset for LARS1-Leu^{syn}, LARS1-ATP^{syn}, LARS1-Leu-AMS^{syn}, and $LARS1^{methyl}$-Leu-AMS^{syn} were collected at 1.0000 Å.

Structure determination

The images were indexed, integrated, and scaled using HKL2000 (Otwinowski and Minor, 1997). Initial phases were obtained by molecular replacement (MR) using the structure of leucyl-tRNA synthetase from *Pyrococcus horikoshii* (PDB 1WKB) as an initial model which is performed by Phaser (Murshudov et al., 1997). Then, density modification including averaging and solvent flipping was conducted using Solomon in CCP4i Suite, followed by automated model building based on the density-modified data with Autobuild module in PHENIX (Adams et al., 2002). The remaining residues were built manually using Coot (Emsley and Cowtan, 2004). The ambiguous atomic positions of residues that resulted from poor electron density of low-resolution data were revised using Morph module in PHENIX, and then, the refinement was conducted using Refine module in PHENIX. Initially, the electron density of the RBD was not clearly shown in the other crystal forms except for the $LARS1^{methyl}$-Leu-AMS^{syn} structure. Therefore, we built the RBD model building based on the X-ray data of $LARS1^{methyl}$-Leu-AMS^{syn}. Data collection and refinement statistics are provided in Table S1. Ramachandran plot of LARS1-Leu^{syn} showed 82% favored, 17% allowed, and 1% outlier regions. Ramachandran plot of LARS1-ATP^{syn} showed 81% favored, 18% allowed, and 1% outlier regions. Ramachandran plot of LARS1-Leu-AMS^{syn}

showed 88% favored, 10% allowed, and 2% outlier regions. Ramachandran plot of LARS1^{methyl}-Leu-AMS^{syn} showed 97% favored, 3% allowed, and 0% outlier regions.

Binding affinity measurement by microscale thermophoresis (MST)

MST assays were performed with a Monolith NT.115 instrument (NanoTemper Technologies) (Bartoschik et al., 2018; Wienken et al., 2010). Each titration curve contained 16 points prepared by serial dilution of ligands and a constant concentration of the fluorescein-labeled protein. To measure the binding affinity between leucine or ATPαS, and purified LARS1 WT or mutants, proteins were fluorescently labeled using a His-Tag Labeling Kit (The Monolith His-Tag Labeling Kit RED-tris-NTA 2nd Generation; NanoTemper Technologies). 10 mM leucine or ATPαS were serially diluted by 2fold 15 times and then the 16 different concentrations of leucine or ATPαS were incubated with labeled LARS1 WT or mutants, which were prepared at 400 nM. Experiments were performed in Tris buffer supplemented with 0.05% (w/v) Tween-20 and 0.05% BSA. The samples were loaded into high precision capillaries (Monolith NT.115 Capillaries; NanoTemper Technologies). MST assays were performed with 80% LED power using a green filter and a 40% MST power. The normalized fluorescence readings (thermophoresis plus T-jump) were plotted as a function of analyte concentration, and the curve fitting and dissociation constant K_d calculation were performed with NanoTemper software. MST assays of leucine to LARS1 and LARS1 mutants under the condition of 1 mM ATPαS were also measured by same method with LARS1-leucine as described above.

Leucine starvation and stimulation of cells

For leucine starvation, cells were rinsed twice with leucine-free DMEM and incubated in leucine-free DMEM for 1 hr. The cells were re-stimulated by the addition of DMEM containing the indicated concentrations of leucine for 10 min.

GTP-agarose pull down assay

After cells were rinsed in ice-cold PBS, cells were collected in GTP-binding buffer (20 mM Tris-HCl (pH 7.5), 5 mM $MgCl_2$, 2 mM PMSF, 20 μg/ml leupeptin, 10 μg/ml aprotinin, 150 mM NaCl and 0.1% Triton X-100). The soluble fraction of the cells was obtained by sonication for 15 s and then centrifugation at 13,000 *g* for 10 min at 4°C. Protein extracts were incubated with GTP-agarose beads for 30 min at 4°C. Beads were then washed with GTP binding buffer, and the supernatant was retained. The retained supernatant was incubated with washed beads for another 30 min. The beads were washed again, then incubated with the retained supernatant overnight at 4°C. After washing five times with GTP binding buffer, GTP-bounded protein extracts were denatured with sample buffer (Lee et al., 2018).

Leucine binding assay

To measure leucine bound to proteins, HEK293T cells were transfected with the indicated cDNAs and empty vector (EV). The cells lysates were pre-cleared with protein G agarose for 1 hr at 4°C and then immunoprecipitated with anti-Myc antibody and protein G agarose which was pre-blocked with 5% BSA for 4 hr at 4°C. After washed with lysis buffer twice, the beads were washed twice with leucine binding buffer (40 mM HEPES-KOH (pH 7.4), 5 mM ATP, 2.5 mM $MgCl_2$, 50 mM KCl, 5 mM NaCl, 0.01% Triton X-100) and incubated with 10 μM L-[4,5-^{3}H(N)]-leucine for 1 hr on ice with tapping of the tubes every 15 min. The beads were washed three times with wash buffer (40 mM HEPES-KOH (pH 7.4), 2.5 mM $MgCl_2$, 50 mM KCl, 5 mM NaCl, 0.01% Triton X-100) and LARS1-bound [^{3}H] leucine was quantified using a liquid scintillation counter (Beckman Coulter) (Yoon et al., 2020). The average cpm of EV group was subtracted from that of LARS1 WT or mutants overexpressing groups to remove non-specific binding of leucine. The amount of relative leucine bound was calculated by dividing cpm of each value by the average cpm of LARS1 WT.

ATP binding assay

For the ATP-binding assay, HEK293T cells were transfected with the indicated cDNAs and empty vector (EV). The cells lysates were pre-cleared with protein G agarose for 1 hr at 4°C and then immunoprecipitated with anti-Myc antibody and protein G agarose which was pre-blocked with 5% BSA for 4 hr at 4°C. After washed twice with lysis buffer, the beads were washed twice with ATP binding buffer (40 mM HEPES-KOH (pH 7.4), 1 mM L-leucine, 2.5 mM $MgCl_2$, 50 mM KCl, 5 mM NaCl, 0.01% Triton X-100) and incubated with 105 μM [2,8-^{3}H] ATP for 1 hr on ice with tapping of the tubes every 15 min. The beads were washed three times with wash buffer (40 mM HEPES-KOH (pH 7.4), 2.5 mM $MaCl_2$, 50 mM KCl, 5 mM NaCl, 0.01% Triton X-100) and [^{3}H]ATP bound was measured using a liquid scintillation counter (Yoon et al., 2020). The average cpm of EV group was subtracted from that of LARS1 WT or mutants overexpressing groups to remove non-specific binding of ATP. The amount of relative ATP bound was calculated by dividing cpm of each value by the average cpm of LARS1 WT.

Isothermal titration calorimetry (ITC)

To measure the dissociation constant (K_d) of leucine to LARS1, ITC experiments were performed using an Affinity ITC (TA Instruments). 0.2 mM of LARS1 in buffer (20 mM Tris, pH 7.5, 150 mM NaCl, 0.1% Tween) was titrated with 2.5 mM of leucine in a syringe. Twenty successive injections of 2.5 μL of leucine were performed to 170 μL of LARS1 in the sample cell. The exact K_d value and stoichiometry of leucine to LARS1 were calculated using NanoAnalyze program but the first injection was not used for the calculation. The K_d value and stoichiometry of leucine to LARS1 in the presence of 1 mM ATPαS were also measured by the same method with the

interaction between LARS1 and leucine as described above. In this case, 0.2 mM of LARS1 in buffer B (20 mM Tris, pH 7.5, 150 mM NaCl, 0.1% Tween, 1 mM ATPαS) was titrated with 2.5 mM of leucine in syringe.

Inflection temperature (T_i) measurement

Prior to T_i measurement, each of leucine, isoleucine, valine, tryptophan were incubated with LARS1 WT, respectively, to compare the stability of LARS1 which was complexed with various ligands. A T_i measurement was performed using Tycho NT.6 (Nanotemper) and calculated by plotting the first derivative of the 350 nm/330 nm ratio to temperature.

Circular dichroism spectroscopy

Far-UV circular dichroism spectra were obtained using a J-715 spectropolarimeter (JASCO) at Korea Basic Science Institute. Circular dichroism measurements were performed at 25°C using a quartz cell with a path length of 1 mm. The protein samples were prepared at 0.1 mg/ml in PBS or in PBS containing 0.2 mg/ml leucine and 0.1 mg/ml ATPαS. The spectra were recorded from 260 nm to 190 nm, averaged five scans. Data were recorded at a scan speed of 100 nm/min, bandwidth of 1.0 nm, 1 s response and 0.1 nm resolution. Near-UV circular dichroism measurements were performed at 25°C using a quartz cell with a path length of 10 mm. The protein samples were prepared at 1 mg/ml in PBS or in PBS containing 2 mg/ml leucine and 1 mg/ml ATPαS. The spectra were recorded from 350 nm to 250 nm, averaged five scans. Data were recorded at a scan speed of 100 nm/min, bandwidth of 1.0 nm, 1 s response and 0.1 nm resolution.

Thermal shift assay

The thermal shift assay was performed using Tycho NT. 6 (NanoTemper Technologies, Munich, Germany). LARS1 proteins were prepared a buffer containing 20 mM Tris-HCl (pH7.5), 150 mM NaCl. To clearly compare the change of thermal shift with various mutants, we used the unfolded LARS1 WT as control protein which was boiled at 100°C in aqueous solution for 1 min. Samples of 10 μL LARS1 constructs at a concentration of 1 mg/ml were prepared in the above buffer, and then loaded into glass capillaries (NanoTemper) by capillary action. Intrinsic fluorescence was recorded at 330 nm and 350 nm while heating the sample from 35–95 °C at a rate of 3 °C/min. The ratio of fluorescence (350/330 nm) and the T_i were calculated by Tycho NT. 6.

QUANTIFICATION AND STATISTICAL ANALYSIS

Quantification of immunoblot images was performed using Multi Gauge V3.0 (Fujifilm). Statistical analysis was performed using Prism 9 (GraphPad) including One-way ANOVA and Two-way ANOVA. Bar graphs were plotted as mean ± SEM P-values < 0.05 were considered statistically significant.